

## 3D Reconstruction of the Tree Internal Decay Based on Radar Waves

Meng Li,<sup>a</sup> Yong Xiang Kang,<sup>a,\*</sup> Van Quy Nguyen,<sup>a,b</sup> Xu Zhen Gao,<sup>c</sup> Li Li Zhang,<sup>a</sup> Jin Ling Wang,<sup>a,d</sup> Xiao Qiang Zhou,<sup>a</sup> and Gang Zhen Ma<sup>a</sup>

TRU Tree Radar is a new tool for the non-destructive testing of trees. In this work, two-dimensional images of the internal defect cross-section of a tree were reconstructed to provide a theoretical basis for accurately judging the shape and position of the internal decay, rationally using wood, and improving the utilization rate of wood. Two-dimensional images of different height defect sequences of tree trunk obtained by TRU tree radar were preprocessed and interpolated. Finally, the three-dimensional reconstruction of internal defects of tree trunk was realized by the surface rendering method and volume rendering method under the Matlab environment. The surface rendering displayed the rough 3D model quickly and effectively. However, the important internal information was incomplete, and the reconstructed model was not intuitive. Volume rendering was used to process each voxel in the data set, so as to describe the physical reality of the internal defects of the tree relatively accurately. An algorithm was proposed to improve the visualization level of internal defects, which can enhance the understanding of the three-dimensional image.

DOI: 10.15376/biores.17.4.6277-6292

Keywords: Tree decay; TRU tree radar; Surface rendering; Volume rendering; 3D reconstruction

Contact information: a: College of Forestry, Northwest A&F University, Yangling, Shaanxi 712100, China; b: Vietnam National University of Forestry – Southern Campus, Trang Bom, Dong Nai 810000, Vietnam; c: Taiyuan Institute of Cultural Relics Protection, Taiyuan, Shanxi 030025, China; d: College of Forestry, Beihua University, Jilin, Jilin 132013, China; \*Corresponding author: yxkang@nwsuaf.edu.cn

### INTRODUCTION

The internal decay of trees is a common natural phenomenon. Trees are affected by adverse environmental factors or attacked by various diseases and insect pests in the natural environment; also, there are physiological reasons for decay (Li *et al.* 2017; Xiao *et al.* 2018). This early stage of the process usually starts from the inside. Although some trees still grow typically, their xylem may have become hollow or decayed (Kang 2019). Interior defects reduce the quality of wood, resulting in loss and waste of forest resources. There are many methods for non-destructive testing of wood, including the computed tomography (CT) scanning method, infrared method, ultrasonic method, mechanical stress wave, shock stress wave, vibration method, radar wave method, and impedance method (Schad *et al.* 1996; Nicolotti *et al.* 2003; Deflorio *et al.* 2008; Arciniegas *et al.* 2014; Allison and Wang 2015; Wu *et al.* 2018). TRU tree radar is a new non-destructive testing tool with many advantages such as no damage, high safety, convenient operation, and simple analysis. Liu (2017) used tree radar to investigate the internal defects of *Platyclusus orientalis* in the Huangdi Mausoleum and studied the law of defects. Li *et al.* (2018)

estimated the relative dielectric constant using Hilbert transform algorithm and reflection amplitude based on radar wave detection; they extracted the trunk profile data by point cloud data technology, which significantly improved the accuracy of radar wave detection. Chen *et al.* (2017) used radar waves to detect and quantitatively evaluate the internal cavity of *Pinus massoniana*. Alani *et al.* (2020) used radar waves to evaluate the internal structure of the trunk and proposed a new method for locating internal defects.

Three-dimensional reconstruction technology can help to obtain three-dimensional structure information from the two-dimensional sequence images of trunk defects and presents a realistic three-dimensional graph (Dong and Ke 2019). Observing and analyzing the trunk's internal defects from multi-angles and levels is convenient, which improves the accuracy and scientific validity of the study and its practical application. Bhandarkar *et al.* (1999, 2006) proposed a CATALOG system that detects and classifies critical defects in logs and reconstructs them by analyzing CT or computerized axial tomography (CAT) images. After that, a new feature-based tracking method was proposed for CT images to detect, locate and reconstruct internal defects in logs. Zhang and Sun (2008) used CT scanned tree sectional images to perform 3D reconstruction of the tree internal decay structure through the MATLAB toolbox. Zhang *et al.* (2010) realized the 3D reconstruction of log defect CT image and implemented virtual processing. Researchers tried a more efficient non-contact remote and near-end sensing method to reconstruct tree trunks and their internal defects in recent years. For example, Berveglieri *et al.* (2017) used vertical optical scanning and panoramic vision to reconstruct the tree trunk. Putman *et al.* (2018) used voxelized terrestrial lidar data to reconstruct the tree model to detect and quantify the structural loss of standing dead trees. Zhang and Khoshelham (2020) proposed a reconstruction method by combining structure from motion (SfM) photogrammetry and acoustic tomography to determine the internal wood quality. Puxeddu *et al.* (2021) used close photogrammetry (CPR) and three-dimensional ultrasound to reconstruct the internal decay of a living adult holm oak. These methods can directly show the volume of wood defects and quantitatively understand the three-dimensional distribution of attenuation.

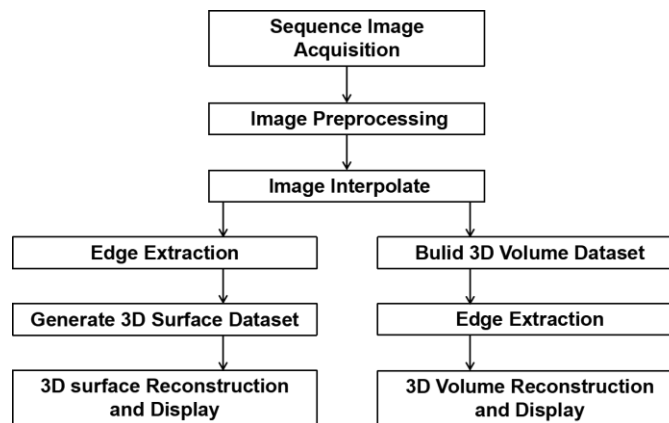


**Fig. 1.** The research framework of the 3D reconstruction process

3D reconstruction technology is relatively mature, and there has been much research in reconstruction algorithms, image processing, *etc.* The research relates to three-dimensional reconstruction of sectional images of internal defects in tree trunks and is mainly focused on CT scanning images. However, from the reconstruction, the

performance of the internal defect areas is not intuitive, and sometimes it is necessary to go through further image segmentation to observe the internal decay areas, which dramatically increases the workload.

At present, research on TRU tree radar is focused on the identification and evaluation of defects and the improvement of detection accuracy. The two-dimensional image of the trunk parsed by different non-destructive testing equipment contains additional internal information, so the image processing methods are different. This paper reconstructs the decay inside the trunk according to the TRU tree radar scan image. The research framework is shown in Fig. 1.

## EXPERIMENTAL

### Materials

The TRU tree radar system is composed of a TerraSIRch™ ground penetrating radar system (Nashua, NH, USA), SIR-3000 (Subsurface Interface Radar) host, and 900 MHz (Model: 3101D) radar signal transmitting system. The radar image analysis software is TreeWin (TreeRadar Inc., Silver Spring, MD, USA) program. Using the TRU tree radar to scan trees includes two independent steps: field data collection and radar wave data analysis.

When TRU tree radar detects trees, the integrated radar transceiver antenna transmits high-frequency electromagnetic waves. In the process of radar wave propagation in the tree trunk medium, when it encounters decay and holes with electrical differences, the electromagnetic wave will be reflected and accepted by the receiving antenna, thereby realizing the process of non-destructive testing (Fig. 2a). The basic principle of detecting wood defect location by radar wave is to obtain the location of a wood defect according to the reflection time and propagation velocity of radar wave at the interface between healthy wood body and defective medium (Fig. 2b). Therefore, the key to defect detection is to determine the propagation and echo time of radar wave in different wood structure layers, and the second is to determine the propagation velocity of an electromagnetic wave in healthy wood body. If the dielectric constant of each wood structure layer is known, then the propagation speed of the electromagnetic wave in the medium is calculated as follows (Xu *et al.* 2012),

$$v = \frac{c}{\sqrt{\varepsilon}} \quad (1)$$

where  $v$  is the propagation velocity of electromagnetic wave in medium (m/ns),  $c$  is the propagation velocity of electromagnetic wave in vacuum = 0.3m/ns, and  $\varepsilon$  is the dielectric constant.

The transceiver antenna in the equipment is integrated, so the  $h$  value in Fig. 2b is approximately equal to  $hI$ , then the formula for calculating the defect location is,

$$h = \frac{v * t}{2} \quad (2)$$

where  $h$  is the defect position,  $v$  is the electromagnetic wave propagation velocity in the medium (m/ns), and  $t$  is the radar wave two-way time at the interface between the healthy wood body and the defect (ns).

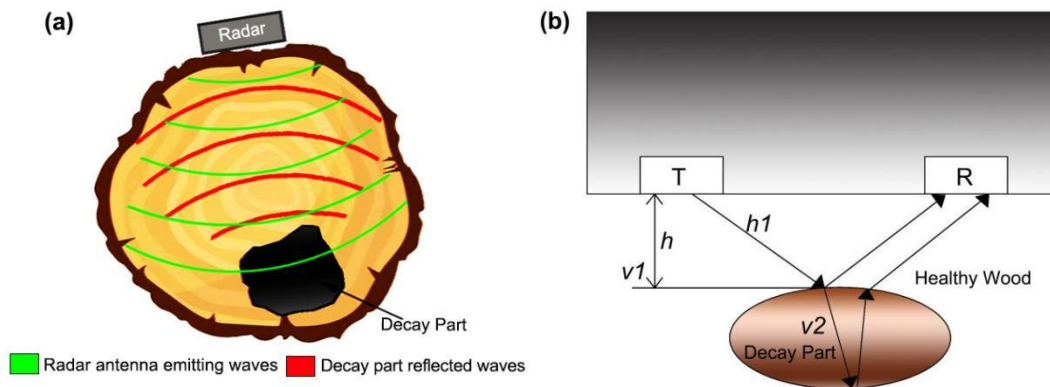


**Fig. 2.** Principle of radar wave detection and defective position detection. (a): Radar wave detection principle; (b): Detection principle of wood defect location, T is the transmitting antenna, R is the receiving antenna,  $h$  is the distance from the bark to the interface between the healthy wood body and the defective medium,  $h1$  is the propagation distance of the radar wave in front of the boundary between the healthy wood body and the defective medium,  $v1$  is the propagation velocity of the radar wave in the healthy wood, and  $v2$  is the propagation velocity of the radar wave in the defect.

This study takes the cedar (*Cedrus deodara*) in Shaanxi Province, China, as the empirical data collection object. During experimental data collection, scanning was carried out from the bottom to the top of the trunk, with positions corresponding to different heights. Radar wave data was obtained at ten heights within 1 m of the tree, and TreeWin software was used to analyze the radar wave data. The B-scan image of the tree trunk is shown in Fig. 3. The horizontal axis represents the distance along the perimeter of the trunk, the vertical axis indicates the depth of entering the trunk, and the green line represents the front surface (bark-wood). A white box is for the analysis gate; after filtering and grain processing, the waveform of the reflected wave and the corresponding internal abnormal characteristic form was reflected clearly. Red “hits” are reflections breaking the threshold and indicate a defect area. Finally, a two-dimensional image corresponding to the height of the tree trunk decay was generated (Fig. 4).

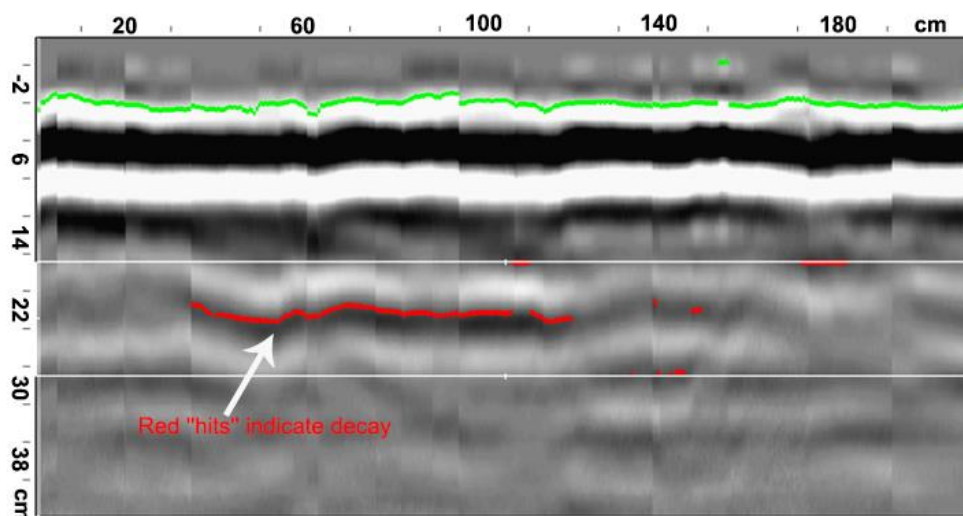


**Fig. 3.** B-scan display

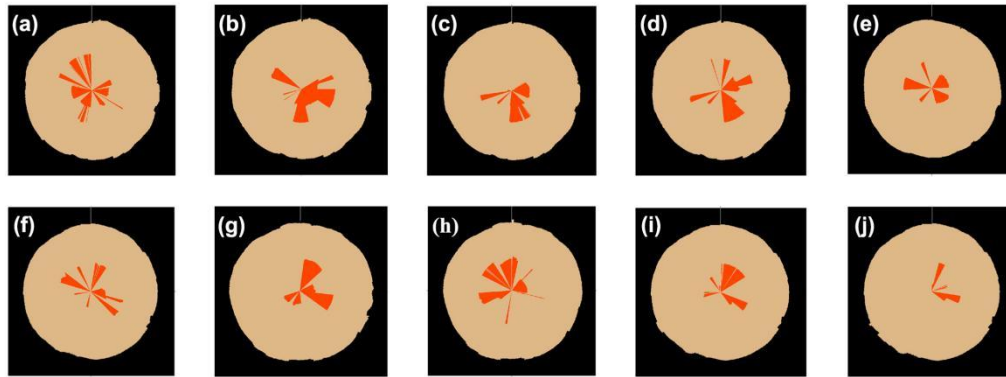


**Fig. 4.** 2D image of tree decay sequence, (a-j) are the internal defect tomographic images of the trunk at 10, 20, 30, 40, 50, 60, 70, 80, 90, and 100 cm

### Gray-Scale Image

To avoid the inconsistency of the detector or the inconsistency of time caused by the uneven imaging of the tomography and the classification of the position and grayscale information between these two-dimensional images in the subsequent three-dimensional reconstruction process, the weighted average method was used for image grayscale processing as follows (Lu 2003; Liu *et al.* 2018).

$$R = G = B = 0.30R + 0.59G + 0.11B \quad (3)$$

where  $R$ ,  $G$ , and  $B$  represent the three primary colors of red, green, and blue, respectively.

### Image Enhancement

Based on image grayscale, the image was enhanced by the linear grayscale method, and the pixel values of the image were transformed by the specified linear function to enhance the gray level and improve the overall contrast of the image (Quan and Wang 2017). If  $x$  is the original gray-scale value, then the changed gray-scale value  $y$  is,

$$y = kx + d (0 \leq y \leq 255) \quad (4)$$

where  $k$  is the degree of inclination and  $d$  is the slope of the linear function on the  $y$ -axis.

According to the morphology of each internal information and whether the interrelationship between them was clearly reflected, the image grayscale and image enhancement processing effect was used to evaluate the advantages and disadvantages of the image with a person as an observer, so there was no general quantitative standard (Su 2007; Sheng and Gong 2019).

### Image Interpolation

Unlike the scanning equipment such as CT, the image data obtained by TRU tree radar scanning is more affected by the uncontrollable factors of the detection equipment and the operators on the data acquisition site. The distance between two adjacent tomographic images is much larger than the distance between two adjacent pixels in the same tomographic image. Inevitably there is data loss, so the reconstructed 3D model is quite different from the real object. Therefore, it is necessary to interpolate the area between the upper and lower layers of the trunk defect tomography image. Linear interpolation was used to interpolate between original images, generate new transition images, and perform

a second interpolation between the interpolated image and the original image to solve the problem of large image spacing and obvious staircase phenomenon.

Suppose that  $S_k(x_i, y_i, z_k)$  and  $S_{k+1}(x_i, y_i, z_{k+1})$  represent two images to be interpolated,  $S_{k+d}(x_i, y_i, z_{k+d})$  represents the intermediate image to be constructed by inter-layer interpolation, and linear interpolation is used. Meanwhile,  $p_k$  and  $p_{k+1}$  represent two corresponding points on  $S_k$  and  $S_{k+1}$ , respectively, then the gray value  $f(p_{k+d})$  of the corresponding point  $p_{k+d}$  on  $S_{k+d}$  is:

$$f(p_{k+d}) = (1-d)f(p_k) + df(p_{k+1}) \quad (5)$$

### Surface Rendering Method

The surface drawing method is a method that generates the intermediate geometric unit by extracting the isosurface of the 3D volume data of the image sequence. Then they were reproduced by traditional computer graphics technology (Li 2008). There are many algorithms for surface drawing. The difference between the algorithms lies in the different geometric units used to approximate the surface or the selection of geometric unit scales. Currently, the most used algorithm is the triangle as the fitting unit. When using the connected outline method for surface drawing, the image is first divided into several characteristic regions by “Canny” edge detection differential operator (Xia *et al.* 2017), and then the contours of each layer are extracted. Finally, the contours of each layer are connected by triangles with the points on the contour lines as vertices to piece together the object surface (Liu 2006).

### Volume Rendering Method

The volume rendering method assigns a certain brightness and opacity to the voxel and then uses the optical principle to project it onto the plane. The basic principle of 3D reconstruction by volume rendering begins with constructing an idealized physical vision model according to the principle of visual imaging; that is, each voxel is a particle, which can transmit, emit, and reflect light. According to the gradient, the light intensity of each data point is calculated, accumulating the translucent color value of each data projected to the same pixel on the image plane. From the initial processing, the results get a processed image (Levoy 1988). Assuming that the light propagates in the  $\vec{\omega}$  direction at the  $r$  point in the volume data, and the direction range is  $S^2$ , the brightness formula is (Deng *et al.* 2012) as follows,

$$\vec{\omega} \times \nabla L(r, \vec{\omega}) = -\phi_l(r, \vec{\omega}) + \varepsilon(r, \vec{\omega}) + \int_{S^2} k(r, \vec{\omega}' \rightarrow \vec{\omega}) L(r, \vec{\omega}') d\omega' \quad (6)$$

where  $\phi_l(r)$  is the absorption coefficient,  $\varepsilon(r, \vec{\omega})$  is the scattering equation, and  $k(r, \vec{\omega}' \rightarrow \vec{\omega})$  is the scattering nucleus.

The specific steps for 3D reconstruction by volume rendering under the MATLAB environment are described below.

#### Construct the 3D volume dataset

First, the “imread” function was used from the MATLAB toolbox to read the existing ten original images and the 27 images obtained by secondary interpolation. Then processed images were used to create a 3D volume dataset D by the “cat” function with a size of  $X \times Y \times 37$ .

### *Preprocessing of reconstruction data*

The volume data set was constructed by the volume drawing method to reduce the display speed and improve the data capacity (Xu *et al.* 2001). The “reducevolume” function was used to delete some data points or fragments with less impact on the graphic display to reduce the data capacity, and the “smooth” function was used to smooth the data to improve the efficiency of the graphical display.

### *Drawing of three-dimensional contours*

The “isosurface” function was used to calculate the cumulative projection of the dataset on the display plane, and the “patch” function was used to create a patch graphics object, this object is one or more polygons determined according to its vertex coordinates. (Zeng *et al.* 2004).

### *Transparency setting and result display*

To ensure that the reconstructed effect can see the position and shape of the decay inside the tree, it is necessary to change the transparency of the patch constructed by the “patch” function to meet the visualization requirements. The transparency value is called the alpha value. To ensure that the reconstructed effect can see the position and shape of the decay inside the tree, it is necessary to change the transparency of the patch constructed by the “patch” function to meet the visualization requirements. Under the MATLAB environment, the “alpha” function was used to set the transparency of all filled images and surface objects within the current coordinate range, by specifying a transparency value between 0 (completely transparent) and 1 (completely opaque). After the transparency was defined, the “lighting” function was used to determine the distribution of the display light on the image, the “view” function was used to define the viewer’s perspective, and finally, the “axis” function was used to define the axis of the displayed image.

## RESULTS AND DISCUSSION

### Image Gray-Scale

The result of the weighted average algorithm to gray-scale the image is shown in Fig. 5. After graying by this method, the image had suitable brightness and darkness, and the edges were clear. The degraded part was different from the benign part, and the overall image contrast was high, which was convenient for further image enhancement.



**Fig. 5.** Gray-scale results. (a) The original image and (b) gray-scale image

### Image Enhancement

Using the gray linear method to adjust the value range of  $k$  and  $d$ , the image enhancement effect was different. Compared with the original image (Fig. 6a), when the

$k > 1$ , the overall effect was enhanced. The decayed part was different from other parts, with an unmistakable edge outline, and there was an apparent difference between black and white (Fig. 6b). In the histogram, the probability of the gray level corresponding to black, white, and gray color was high (Fig. 6b1). When  $0 < k < 1$ , the contrast and brightness of the image decreased. The overall effect was weakened, and the edge of defect was not apparent (Fig. 6c). The corresponding histogram shows that the gray distribution was mainly concentrated in one region (Fig. 6c1). When  $k = 1$ , the image was the original image. When  $k = 1$ ,  $d > 0$ , it shows the increase of image brightness (Fig. 6d). The change of  $d$  value shifts the overall gray distribution of the corresponding histogram to the right (Fig. 6d1). When  $k < 0$ , it shows the reverse display effect (Fig. 6e). Comparing the four value ranges, the best enhancement effect was at  $k > 1$  when using the gray-scale linear method for image contrast.

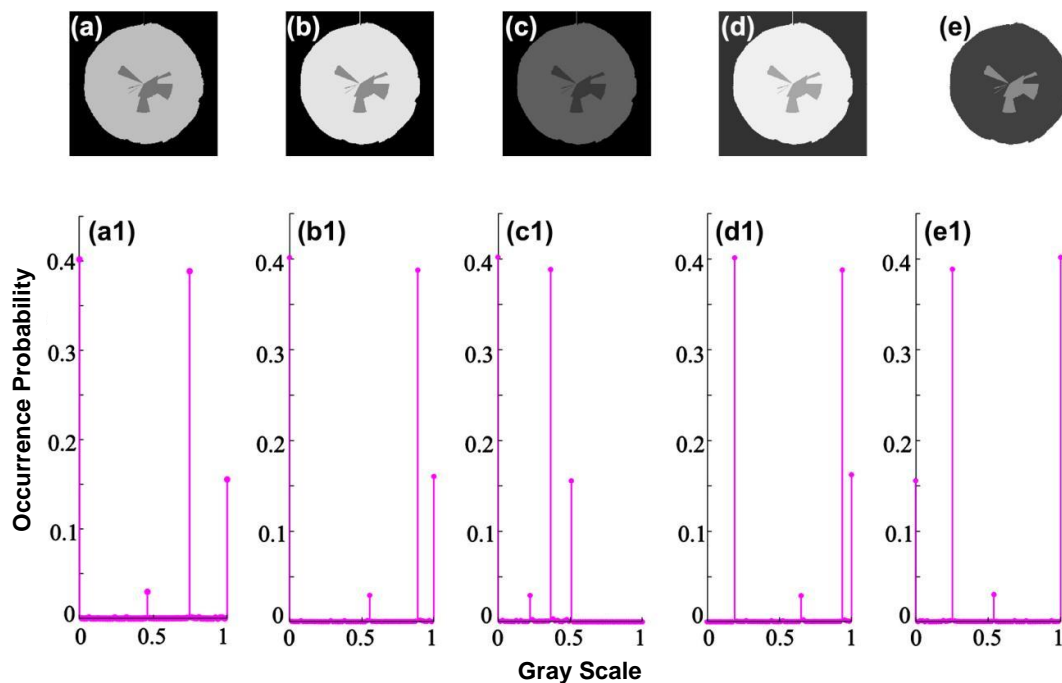


**Fig. 6.** Contrast adjustment and corresponding histogram, (a), (a1): original images; (b), (b1):  $k=1.3$ ,  $d=0$ ; (c), (c1):  $k=0.5$ ,  $d=0$ ; (d), (d1):  $k=1$ ,  $d=50$ ; (e), (e1):  $k=-1$ ,  $d=255$

### Image Interpolation

Figure 7 shows the result of image interpolation using linear interpolation. Figures 7a and 7b are the upper and lower layer images ready for interpolation. After the first interpolation, the difference between the interpolated image and the upper and lower layer images was still significant. The step phenomenon was evident, and the effect was not ideal (Fig. 7c). After the second inter-layer interpolation, the difference between the upper and lower layer images was less pronounced, and the interpolated image was similar to the upper and lower layer images (Fig. 7f), which achieved a good transition. The interpolation of sequential sectional images will increase the number of sequential images and it can improve the accuracy of subsequent 3D reconstruction. Because the sequence image increases the number of images after twice interlayer interpolation, and the image interpolation processing also takes a certain amount of time, finding a suitable interlayer interpolation algorithm improves the speed and accuracy of 3D reconstruction.



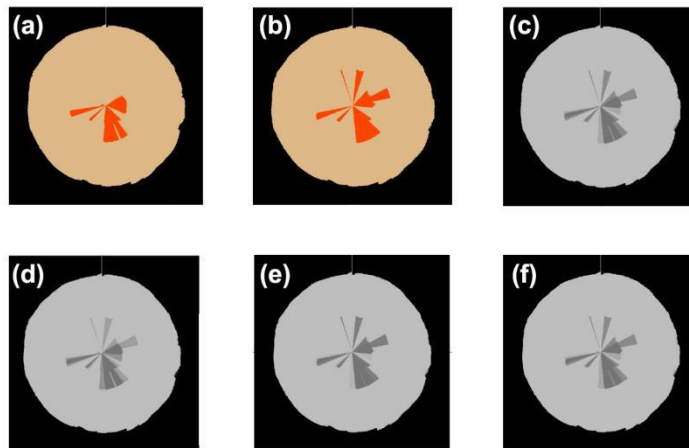


**Fig. 7.** Image Interpolation Results, (a), (b) are the upper and lower layer images to be interpolated, respectively; (c) is the interpolated images obtained by linear interpolation; (d), (e) are the upper and lower layer images obtained by the first linear interpolation; (f) is the interpolated images obtained by the second linear interpolation.

### Surface Rendering

The surface rendering method has higher requirements for edge detection. Figure 8 shows the result of edge detection by a “canny” operator. In the “canny” operator, the high and low thresholds affect the edge results. With a higher threshold, fewer edge points are detected, but the low threshold should not be set too high. Otherwise, some edge information is lost. In order to avoid the problem of poor adaptation caused by manually setting the threshold, this study used the maximum between-class variance (OTSU Method). According to the gray characteristics of the image, the image is divided into the background and foreground of the target object. Then the high threshold and low threshold are obtained. After edge detection using the “canny” operator, the contour of the decay inside the trunk was clear and complete, and the effect was better.

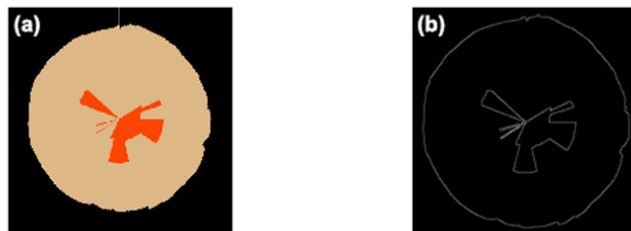


**Fig. 8.** Edge detection result. (a) Original image and (b) edge detection image

Figure 9 shows the surface drawing effect of using the triangle connection formed by the shortest diagonal as the fitting unit and then connecting the contours. When using this method for reconstruction, the correspondence between the contour lines is very critical. If there are more than one contour lines between the two adjacent layers, it is worth considering which contour lines should be connected in the adjacent contour lines. When the change of adjacent contour lines is relatively large, the corresponding difficulty of the contour lines is greater. Therefore, the contour correspondence problem can be effectively solved only by selecting an appropriate interpolation method. On the other hand, the

surface drawing method requires high accuracy of edge detection. The display effect is not good for some images whose features are not obvious. Because the data processed by surface method is only a part of the whole volume of data, the processed data has the advantages of the small calculation amount, small memory occupation, and fast running speed. With the support of computer hardware, it can smoothly carry out 3D interaction. Although the algorithm can reconstruct the decay more quickly, there is limited retention of the internal information, and the displayed information is only superficial information, which is inconvenient for further observation and analysis. Therefore, the physical model can only be restored to a certain extent.

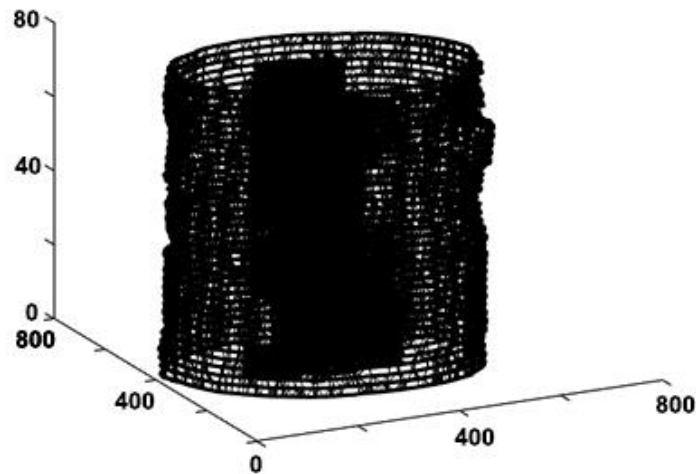
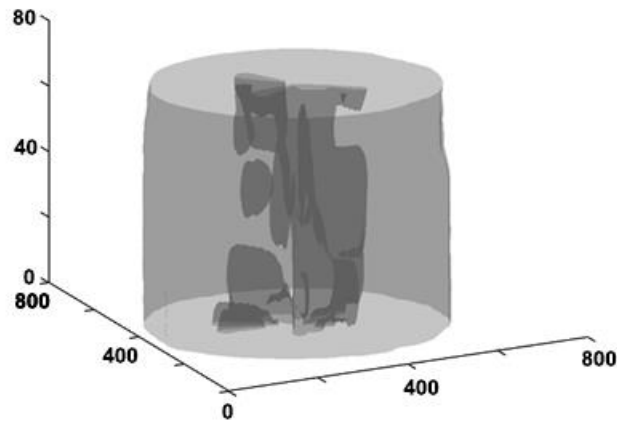


Fig. 9. Surface rendering reconstruction results

### Volume Rendering

Unlike surface rendering, the advantage of volume rendering is that it does not require precise cutting of two-dimensional images. Instead it processes each voxel in the volume data set separately and finally reconstructs a three-dimensional image. Figure 10 shows the result of 3D reconstruction by the volume rendering method. This algorithm can recover the shape of the trunk from the macroscopic analysis, and the introduction of transparency enhances the display effect of the whole image.

After defining the transparency of the attributes of the constructed fragments, it makes the micro details such as the shape and relative spatial position relationship of the internal defects of the trunk more obvious, and the visualization of the whole image becomes higher. The volume rendering algorithm needs to calculate each voxel in the volume data field, so the amount of calculation is relatively large, which reduces the display speed of the image, and the change of the viewing angle of illumination and display will make the whole rendering process start again. This approach is restricted by computer hardware, so it cannot meet the needs of real-time display. Although the speed of using this method to reconstruct is slower than that of the surface reconstruction method, after processing each voxel in the volume data set, more internal information of the trunk is preserved. The details are kept intact, so the reconstructed model is more accurate and convenient for further observation and analysis.



**Fig. 10.** Volume rendering reconstruction results

### **Development and Validation of 3D Visualization System for Decay inside the Tree**

Using surface rendering and volume rendering for 3D reconstruction, the volume rendering method had a better reconstruction effect, and the model had a strong sense of reality. Based on the volume rendering method, a 3D visualization system for decay inside trees was developed that generates a file “.exe” that can run independently. The user does not need to install MATLAB, but directly installs the executive program. The system provides overall functions by menu items. The menu function area includes file reading, model reconstruction, and model export.

After the interface and properties of the program were defined, the callback function was designed corresponding to the menu item and associated its item with the callback function to realize the menu function (Fig. 11a). When using this system, the two-dimensional images of different heights obtained by tree radar are preprocessed, interpolated, and stored in the newly-built folder. After using this system to read the file, the three-dimensional visualization effect of the defect is displayed. In order to verify the effectiveness and reliability of the system and the reconstruction method, this study takes the species *Gleditsia sinensis* as an example to reconstruct (Fig. 11b).

The study tree is located in Xianyang City, Shaanxi Province, China. It is an ancient tree about 300 years old, DBH=135 cm. The tree has serious defects and has formed an open cavity. The internal defect characteristics can be directly observed without cutting, which is convenient for later comparison. Therefore, the method of this study is used to acquire and preprocess the image of the trunk defect at the height of 1 m from the ground, and then the internal defect is reconstructed by this system. From the reconstruction results displayed in the system (Fig. 11a), this method can directly show the shape of the wood defect and quantitatively understand the attenuation volume of the tree, which has certain reliability and authenticity.

Because of various differences in the shapes of the reconstructed objects, it is difficult to have a reconstruction method that can directly reconstruct objects of any shape. Hence, these methods still need to be clarified. Due to the limitation of time and conditions, this research work only involves a small part of all the reconstruction methods, and a lot of work still needs to be further studied and discussed. As far as this study is concerned, it is necessary to continue the research in the following aspects: (i) Continue to study the 3D reconstruction algorithm in depth.



## CONCLUSIONS

1. The information contained in the two-dimensional images obtained by TRU radar scanning was different from that of CT equipment and stress wave equipment, so the processed image method was also different. The linear grayscale method improved the object contrast and solved the problem that the original image gap is too large by a series of two linear interpolations, which lays the foundation for the subsequent 3D reconstruction.
2. Based on two-dimensional image preprocessing and image interpolation of TRU tree radar, the results of 3D reconstruction by surface rendering and volume rendering showed that the surface rendering algorithm reduced the original data to compact surface data. The calculations can run quickly in the MATLAB environment. The study defined the transparency of the patches constructed in the reconstruction process in the volume rendering, which improved the visualization level of microscopic details, such as the shape and position, and did not need to segment. The three-dimensional visualization system of the decay tree was designed with MATLAB/GUI, which gets rid of the problem that the “.m” program cannot run independently without MATLAB, and the reliability and authenticity of the research method and system are verified by an example, which lays a foundation for the popularization and application of 3D reconstruction technology in the field of tree non-destructive testing.

## ACKNOWLEDGMENTS

This research was supported by the National Forestry Public Welfare Industry Scientific Research Project of China (No. 201404302) and the Key Scientific Research Project of Northwest A&F University (No. Z109021310). The authors thank Prof. Dr. Kang Yong Xiang, Dr. Nguyen Van Quy, Dr. Zhang Li Li and Dr. Wang Jin ling, and the research team of Northwest A&F University, China, for their valuable assistance during the preparation of the manuscript.

## REFERENCES CITED

- Alani, A. M., Giannakis, I., Zou, L. L., Lantini, L., and Tosti, F. (2020). “Reverse-time migration for evaluating the internal structure of tree-trunks using ground-penetrating radar,” *NDT & E International* 115, article no. 102294. DOI: 10.1016/j.ndteint.2020.102294
- Allison, R. B., and Wang, X. P. (2015). *Nondestructive Testing in the Urban Forest*, USDA Forest Service, Forest Products Laboratory, Madison, WI, USA.
- Arciniegas, A., Prieto, F., Brancheriau, L., and Lasaygues, P. (2014). “Literature review of acoustic and ultrasonic tomography in standing trees,” *Trees* 28(6), 1559-1567. DOI: 10.1007/s00468-014-1062-6
- Berveglieri, A., Tommaselli, A. M. G., Liang X. L., and Honkavaara, E. (2017). “Vertical optical scanning with panoramic vision for tree trunk reconstruction,” *Sensors* 17(12), article no. 2791. DOI: 10.3390/s17122791
- Bhandarkar, S. M., Faust, T. D., and Tang, M. J. (1999). “CATALOG: A system for

- detection and rendering of internal log defects using computer tomography,” *Machine Vision and Applications* 11(4), 171-190. DOI: 10.1007/s001380050100
- Bhandarkar, S. M., Luo, X. Z., Daniels, R., and Tollner, E. W. (2006). “A novel feature-based tracking approach to the detection, localization, and 3-D reconstruction of internal defects in hardwood logs using computer tomography,” *Pattern Analysis & Applications* 9(2), 155-175. DOI: 10.1007/s10044-006-0035-9
- Chen, Y., Gao, T., Li, D., and Guo, W. (2017). “Detection and quantitative evaluation of internal cavity of *Pinus massoniana* wood by radar testing technology,” *Scientia Silvae Sinicae* 53(10), 139-145. DOI: 10.11707/j.1001-7488.20171015
- Deflorio, G., Fink, S., and Schwarze, F. (2008). “Detection of incipient decay in tree stems with sonic tomography after wounding and fungal inoculation,” *Wood Science & Technology* 42(2), 117-132. DOI: 10.1007/s00226-007-0159-0
- Deng, S. L., Zhang, L. Y., Shi, Y., Quan, S. H., and Wen, J. (2012). “3D reconstruction of porous materials based on volume rendering,” *Journal of Wuhan University of Technology (Information & Management Engineering)* 34(1), 42-45. DOI: 10.3963/j.issn.1007-144X.2012.01.012
- Dong, P. H., and Ke, L. J. (2019). “Overview of 3D reconstruction techniques based on images,” *Radio Communications Technology* 45(2), 115-119. DOI: CNKI: SUN: WXDT.0.2019-02-001
- Kang, Y. C. (2019). *Study on the Law of Hollow Corruption of Ancient *Platycladus orientalis* Based on TRUtree Radar*, Master’s Thesis, Northwest Agriculture & Forestry University, Shaanxi, China.
- Levoy, M. (1988). “Display of surfaces from volume data,” *IEEE Computer Graphics and Applications* 8(3), 29-37. DOI: 10.1109/38.511
- Li, W. L., Wen, J., Xiao, Z. L., Zhang, J., and Han, H. Y. (2017). “Detection of internal anomaly for trees in the Summer Palace based on radar,” *Journal of Fujian Agriculture and Forestry University (Natural Science Edition)* 46(6), 665-671. DOI: 10.13323/j.cnki.j.fafu(nat.sci.).2017.06.011
- Li, W. L., Wen, J., Xiao, Z. L., Xu, S. X. (2018). “Application of ground-penetrating radar for detecting internal anomalies in tree trunks with irregular contours,” *Sensors* 18(2), 649. DOI: 10.3390/s18020649
- Li, X. Y. (2008). *Research and Implement of the 3D Surface Reconstruction*, Master’s Thesis, Central South University, Hunan, China.
- Liu, G. (2006). *Study on Reconstruction form a Collection of Planar Contours*, Master’s Thesis, Shandong University of Science and Technology, Jinan, China.
- Liu, M., Xue, X. S., Liu, G. W., Liu, Z., and Cai, H. (2018). “Color to grayscale algorithm based on local contrast enhancement in contourlet transform domain,” *Journal of Changchun University of Science and Technology (Natural Science Edition)* 41(5), 70-74. DOI: 10.3969/j.issn.1672-9870.2018.05.017
- Liu, X. D., Kang, Y. X., Gan, M. X., Li, X. J., and Liu, W. (2017). “A study on trunk decay of ancient *Platycladus orientalis* in tomb of yellow emperor,” *Journal of Northwest Forestry University* 32(2), 180-187. DOI: 10.3969/j.issn.1001-7461.2017.02.31
- Lu, J. B. (2003). “A new encoding method for bitmap and its applications,” *Computer Engineering and Applications* 39(34), 102-103. DOI: 10.3321/j.issn:1002-8331.2003.34.034

- Nicolotti, G., Socco, L. V., Martinis, R., Godio, A., and Sambuelli, L. (2003). "Application and comparison of three tomographic techniques for detection of decay in trees," *Journal of Arboriculture* 29(2), 66-78. DOI: 10.48044/jauf.2003.009
- Putman, E. B., Popescu, S. C., Eriksson, M., Zhou, T., Klockow, P., Vogel, J., and Moore, G. W. (2018). "Detecting and quantifying standing dead tree structural loss with reconstructed tree models using voxelized terrestrial lidar data," *Remote Sensing of Environment* 209, 52-65. DOI: 10.1016/j.rse.2018.02.028
- Puxeddu, M., Cuccuru, F., Fais, S., Casula, G., and Bianchi, M. G. (2021). "3D Imaging of CRP and ultrasonic tomography to detect decay in a living adult holm oak (*Quercus ilex* L.) in Sardinia (Italy)," *Applied Sciences* 11(3), article no. 1199. DOI: 10.3390/app11031199
- Quan, H. Y., and Wang, C. B. (2017). *Principles and Practices of Digital Image Processing*, China Machine Press, Beijing, China.
- Schad, K. C., Schmoldt, D. L., and Ross, R. J. (1996). *Nondestructive Methods for Detecting Defects in Softwood Logs*, US Department of Agriculture, Forest Service, Forest Products Laboratory, Madison, WI, USA.
- Sheng, X. Y., and Gong, C. (2019). "Research on digital image interpolation algorithm," *Computer Knowledge and Technology* 15(3Z), 4. DOI: 10.14004/j.cnki.ckt.2019.0776
- Su, M. (2007). *Research and Implementation on the 3D Reconstruction Technology of Medical CT Images*, Master's Thesis, Hebei University of Technology, Tianjin, China.
- Wu, X., Li, G. H., Jiao, Z., and Wang, X. P. (2018). "Reliability of acoustic tomography and ground-penetrating radar for tree decay detection," *Applications in Plant Sciences* 6(10), e01187. DOI: 10.1002/aps3.118710.1002/aps3.1187
- Xia, B., Zhang, Y. L., and Wang, F. (2017). "Research of Canny-based image segmentation method of raw cotton impurities," *Advanced Textile Technology* 25(6), 23-26. DOI: 10.19398/j.att.2017.06.005
- Xiao, X. Y., Wen, J., Xiao, Z. L., Li, W. L., and Zhang, H. J. (2018). "Detection and recognition of tree trunk internal structure based on radar," *Scientia Silvae Sinicae* 54(5), 127-134. DOI: 10.11707/j.1001-7488.20180514
- Xu, Y. X., Wu, X. Q., and Hu, Y. J. (2001). "3D rebuilding of biology slice image by volume rendering in MATLAB," *Computer Engineering* 27(12), 114-115. DOI: 10.3969/j.issn.1000-3428.2001.12.044
- Xu, T. J., Ji, W. R., and Fan, F. (2012). "Working principle of ground penetrating radar and its application in tunnel quality inspection," *Engineering and Construction* 26(02), 214-216. DOI: 10.3969/j.issn.1673-5781.2012.02.026
- You, X. F. (2010). *A Preliminary Study on 3D Reconstruction of Inner Decay in Log Cross-section Based on 2D Images of Stress Wave*, Master's Thesis, Northeast Forestry University, Heilongjiang, China.
- Zeng, Z., Dong, F. H., Chen, X., Zhou, H., and Zhou, J. Z. (2004). "Three dimensions reconstruction of CT image by MATLAB," *Computerized Tomography Theory and Applications* 13(2), 24-29. DOI: CNKI: SUN: CTLL.0.2004-02-005
- Zhang, R. N., and Sun, L. P. (2008). "Three dimensions reconstruction of log CT image by MATLAB," *Wood Processing Machinery* 19(4), 24-26. DOI: 10.13594/j.cnki.mcjgjx.2008.04.010

Zhang, X. H., Ye, N., Ding, J. W., and Wang, H. L. (2010). "Investigations of 3D reconstruction of log CT images and imaginary cutting," *Journal of Nanjing Forestry University (Natural Science Edition)* 34(2), 77-80.

DOI: 10.3969/j.issn.1000-2006.2010.02.017

Zhang, J., and Khoshelham, K. (2020). "3D reconstruction of internal wood decay using photogrammetry and sonic tomography," *The Photogrammetric Record* 35(171), 357-374. DOI: 10.1111/phor.12328

Article submitted: May 5, 2022; Peer review completed: Sept. 11, 2022; Revised version received and accepted: September 17, 2022; Published: September 21, 2022.

DOI: 10.15376/biores.17.4.6277-6292